6th European Conference on Computational Mechanics (ECCM 6)
7th European Conference on Computational Fluid Dynamics (ECFD 7)
1115 June 2018, Glasgow, UK

HYBRID RANS-LES SIMULATIONS WITH THE DISCONTINUOUS GALERKIN METHOD

F. Bassi[1], A. Colombo[1], F.C. Massa[1], G. Noventa[2,*] and A. Ghidoni[2]

[1] University of Bergamo, Department of Engineering and Applied Sciences
viale Marconi, 5 - 24044 Dalmine (BG), Italy
{francesco.bassi, alessandro.colombo, francescocarlo.massa}@unibg.it

[2] University of Brescia, Department of Mechanical and Industrial Engineering
via Branze, 38 - 25123, Brescia, Italy
{gianmaria.noventa, antonio.ghidoni}@unibs.it

Key words: discontinuous Galerkin, hybrid RANS-LES, eXtra-LES, compressible flow

Abstract. In recent years, a growing interest has been shown for hybrid RANS-LES approaches and their application to high-fidelity simulations of massively separated flows. Such modelling approach is intended as a way to go beyond the known limitations of the RANS in simulating massively separated flows and the computational cost of LES, which is nowadays still too demanding for a practical use.

The aim of this work is to show recent advancements of the eXtra-Large Eddy Simulation (X-LES) model [1] in the discontinuous Galerkin (DG) solver named MIGALE [2]. The main features of the X-LES formulation are: (i) a clearly defined subgrid-scale (SGS) model based on the k-equation, (ii) a single turbulent kinetic energy equation switching dynamically between the RANS and LES formulations, (iii) the independence of the model from the wall distance.

The LES formulation of the X-LES method has been validated and recalibrated using the decay of homogeneous and isotropic turbulence (DHIT). The sensitivity of the energy spectrum to X-LES model constants and mesh size has been evaluated. The X-LES prediction capabilities have been demonstrated in the computation of external aerodynamic problems with massively separated flows, *i.e.* the flow around a circular cylinder at $\mathrm{Re} = 10^5$ and the shock wave/boundary layer interaction on a swept bump.

1 INTRODUCTION

In recent years an ever-increasing interest to go beyond the limited predictive capability of the Reynolds-averaged Navier-Stokes (RANS) formulation has been shown. In the range of moderate Reynolds numbers, availability of large HPC resources now allows to employ Large Eddy Simulation (LES) also in complex flow applications. In this context, the practice of an implicit LES (ILES) based on the Discontinuous Galerkin (DG) method showed to be very promising due to the good dispersion and dissipation properties of the

method. However, to date, characteristic Reynolds numbers of many industrial applications are too large for a fully resolved LES. For these applications the use of a hybrid RANS-LES model or a wall modelled LES approach seems mandatory.

In hybrid RANS-LES models the RANS equations are active close to solid walls, where LES would be prohibitively costly, while LES is used in regions of separated flow where larger eddies can be resolved. Among the hybrid approaches available in the literature, the eXtra-Large Eddy Simulation (X-LES) method [1, 3] has three attractive features: (*i*) independence from the wall distance; (*ii*) use in LES mode of a clearly defined subgrid-scale (SGS) model [5]; (*iii*) use of the k-ω turbulence model integrated to the wall.

Chapter 2 describes the implementation in MIGALE code of the X-LES method, while in Chapter 3 the LES formulation of the hybrid method has been validated and recalibrated using the decay of homogeneous and isotropic turbulence (DHIT), and the full formulation prediction capabilities have been demonstrated in the computation of external aerodynamic problems with massively separated flows: the flow around a circular cylinder at $\mathrm{Re} = 10^5$ and the shock wave/boundary layer interaction on a swept bump.

2 THE X-LES HYBRID RANS-LES MODEL

The complete set of equations of the X-LES model implementation proposed by Bassi *et al.* in [3, 4] can be written as

$$\frac{\partial \rho}{\partial t} + \frac{\partial}{\partial x_j}(\rho u_j) = 0, \tag{1}$$

$$\frac{\partial}{\partial t}(\rho u_i) + \frac{\partial}{\partial x_j}(\rho u_j u_i) = -\frac{\partial p}{\partial x_i} + \frac{\partial \widehat{\tau}_{ji}}{\partial x_j}, \tag{2}$$

$$\frac{\partial}{\partial t}(\rho E) + \frac{\partial}{\partial x_j}(\rho u_j H) = \frac{\partial}{\partial x_j}\left(u_i \widehat{\tau}_{ij} - \widehat{q}_j\right) - P_k + D_k, \tag{3}$$

$$\frac{\partial}{\partial t}\left(\rho k\right) + \frac{\partial}{\partial x_j}\left(\rho u_j k\right) = \frac{\partial}{\partial x_j}\left[\left(\mu + \sigma^* \bar{\mu}_t\right)\frac{\partial k}{\partial x_j}\right] + P_k - D_k, \tag{4}$$

$$\begin{aligned}\frac{\partial}{\partial t}\left(\rho\widetilde{\omega}\right) + \frac{\partial}{\partial x_j}\left(\rho u_j \widetilde{\omega}\right) = \frac{\partial}{\partial x_j}\left[\left(\mu + \sigma \bar{\mu}_t\right)\frac{\partial \widetilde{\omega}}{\partial x_j}\right] &+ \left(\mu + \sigma\bar{\mu}_t\right)\frac{\partial \widetilde{\omega}}{\partial x_k}\frac{\partial \widetilde{\omega}}{\partial x_k} \\ &+ P_\omega - D_\omega + C_D,\end{aligned} \tag{5}$$

where ρ is the fluid density, E and H the stagnation or total energy and enthalpy per unit mass, respectively, while the pressure p, the mean strain-rate tensor S_{ij}, the turbulent and total stress tensor, $\hat{\tau}_{ij}$ and τ_{ij}, the heat flux vector $\hat{q}_j$ and the limited values of eddy viscosity $\overline{\mu}_t$ are given by

$$p = (\gamma - 1)\rho\left(E - \frac{1}{2}u_k u_k\right), \tag{6}$$

$$S_{ij} = \frac{1}{2}\left(\frac{\partial u_i}{\partial x_j} + \frac{\partial u_j}{\partial x_i}\right), \tag{7}$$

$$\tau_{ij} = 2\overline{\mu_t}\left(S_{ij} - \frac{1}{3}\frac{\partial u_k}{\partial x_k}\delta_{ij}\right) - \frac{2}{3}\rho\overline{k}\delta_{ij}, \qquad \widehat{\tau}_{ij} = 2\mu\left(S_{ij} - \frac{1}{3}\frac{\partial u_k}{\partial x_k}\delta_{ij}\right) + \tau_{ij}, \tag{8}$$

$$\widehat{q_j} = -\left(\frac{\mu}{\mathrm{Pr}} + \frac{\mu_t}{\mathrm{Pr}_t}\right)\frac{\partial h}{\partial x_j}, \tag{9}$$

$$\overline{\mu}_t = \alpha^* \frac{\rho\overline{k}}{\hat{\omega}}, \tag{10}$$

where $\overline{k} = \max(0, k)$. Here γ is the ratio of gas specific heats, Pr and Pr_t are the molecular and turbulent Prandtl numbers. The production, destruction and cross diffusion terms are

$$P_k = \tau_{ij}\frac{\partial u_i}{\partial x_j}, \quad P_\omega = \alpha\left[\alpha^*\frac{\rho}{e^{\widetilde{\omega}_r}}\left(S_{ij} - \frac{1}{3}\frac{\partial u_k}{\partial x_k}\delta_{ij}\right) - \frac{2}{3}\rho\delta_{ij}\right]\frac{\partial u_i}{\partial x_j}, \tag{11}$$

$$D_k = \beta^*\rho\bar{k}\hat{\omega}, \quad D_\omega = \beta\rho e^{\widetilde{\omega}_r}, \quad C_D = \sigma_d\frac{\rho}{e^{\widetilde{\omega}_r}}\max\left(\frac{\partial k}{\partial x_k}\frac{\partial\widetilde{\omega}}{\partial x_k}, 0\right). \tag{12}$$

In this implementation, being k limited to zero, X-LES actually switches between three different flow models: Implicit-LES (ILES), LES with a well defined explicit SGS model [5] and RANS closed by the k-ω model. The automatic switching among the models is obtained through the definition of a "composite" specific dissipation rate

$$\hat{\omega} = \max\left(e^{\widetilde{\omega}_r}, \frac{\sqrt{\overline{k}}}{C_1\Delta}\right), \tag{13}$$

where Δ is the SGS filter width and C_1 a model coefficient. Although in the literature the filter width parameter is often related to the local mesh spacing, here a constant value has been used over the whole computational mesh. A constant value has been also used by Kok [1] for some of the test cases.

The variable $\widetilde{\omega}_r$ in the source terms of Eqs. 4 and 5 and in the "composite" specific dissipation rate definition in Eq. 13 indicates that $\widetilde{\omega}$ must fulfill a suitably defined "realizability" condition, which sets a lower bound on $\widetilde{\omega}$. This constraint ensures that X-LES, regardless of being in RANS or LES mode, predicts positive normal turbulent stresses and satisfies the Schwarz inequality for shear stresses

$$\begin{aligned} &\overline{\rho u_i'^2} \geq 0, \quad i = 1,2,3, \\ &\overline{\rho u_i' u_j'}^2 \leq \overline{\rho u_i'^2}\,\overline{\rho u_j'^2}, \quad i,j = 1,2,3, \quad i \neq j, \end{aligned} \tag{14}$$

where u_i' indicates the fluctuating part of the i-th component of the velocity and the overline symbol the temporal average operator.

Being in X-LES both the Reynolds and the subgrid stress tensor modelled according to the Boussinesq hypothesis, an overall "realizability" condition can be enforced through the definition of a suitably modified specific dissipation rate. In fact, after some algebra, Eqs. 14 can be written in terms of modelled stresses as

$$\frac{e^{\widetilde{\omega}}}{\alpha^*} - 3\left(S_{ii} - \frac{1}{3}\frac{\partial u_k}{\partial x_k}\right) \geq 0, \quad i = 1,2,3, \tag{15}$$

$$\left(\frac{e^{\widetilde{\omega}}}{\alpha^*}\right)^2 - 3\left(S_{ii} + S_{jj} - \frac{1}{3}\frac{\partial u_k}{\partial x_k}\right)\frac{e^{\widetilde{\omega}}}{\alpha^*} \\ +9\left[\left(S_{ii} - \frac{1}{3}\frac{\partial u_k}{\partial x_k}\right)\left(S_{jj} - \frac{1}{3}\frac{\partial u_k}{\partial x_k}\right) - S_{ij}^2\right] \geq 0, \quad i,j = 1,2,3, \quad i \neq j. \tag{16}$$

Let us denote with a the maximum value of the unknown $e^{\widetilde{\omega}}/\alpha^*$ that fulfills the inequalities 15 and 16. The lower bound $\widetilde{\omega}_{r0}$ that guarantees realizable stresses is then given by

$$\frac{e^{\widetilde{\omega}_{r0}}}{\alpha^*} = a. \tag{17}$$

Since in this work the underlaying turbulence model is the high-Reynolds version of k-ω, α^* is constant and the solution of Eq. 17 is trivial. The "realizability" constraint can be finally enforced as

$$\widetilde{\omega}_r = \max\left(\widetilde{\omega}, \widetilde{\omega}_{r0}\right). \tag{18}$$

3 NUMERICAL RESULTS

X-LES equations are here discretized in space according to the DG method, see [3] for details. The accurate high-order time integration is here performed by means of the multi-stage linearly implicit (Rosenbrock-type) Runge-Kutta schemes. In particular, the three stages, order three (ROS3P) scheme of Lang and Verwer [6] has been used. An extended review of several Rosenbrock schemes as well as their coefficients are reported in [7]. The solver relies on PETSc, [9], for the linear solvers and to manage distributed arrays and the communication among them.

3.1 DECAY OF ISOTROPIC TURBULENCE

The decay of homogeneous and isotropic turbulence (DHIT) has been investigated to test the X-LES formulation as pure LES. The numerical results have been compared to the experiment of Comte-Bellot and Corrsin [8]. In the experiment, the turbulence was generated by a grid with mesh size $M = 50.8\,\mathrm{mm}$ and for an inlet velocity $u = 10\,\mathrm{m/s}$. The Reynolds number, based on these scales, is $Re = uM/\nu = 34000$. The energy spectra $E(\lambda, t)$ were measured at three stations along the flow, at positions $42M$, $98M$ and $171M$ from the grid.

As suggested by Kok *et al.* [1], LES describes a filtered velocity field and a proper comparison with the experimental data requires the filtering of the experimental data with the same function. The second-order top-hat filter, which consists of averaging over the filter width in physical space has been adopted and the one dimensional filter function

$$f(\lambda, \Delta) = \frac{\sin\left(\frac{1}{2}\lambda\Delta\right)}{\frac{1}{2}\lambda\Delta}, \tag{19}$$

where $\boldsymbol{\lambda} = \mid \lambda \mid$ and $\Delta = L/32$ has been extended to the three dimensional case by assuming isotropy.

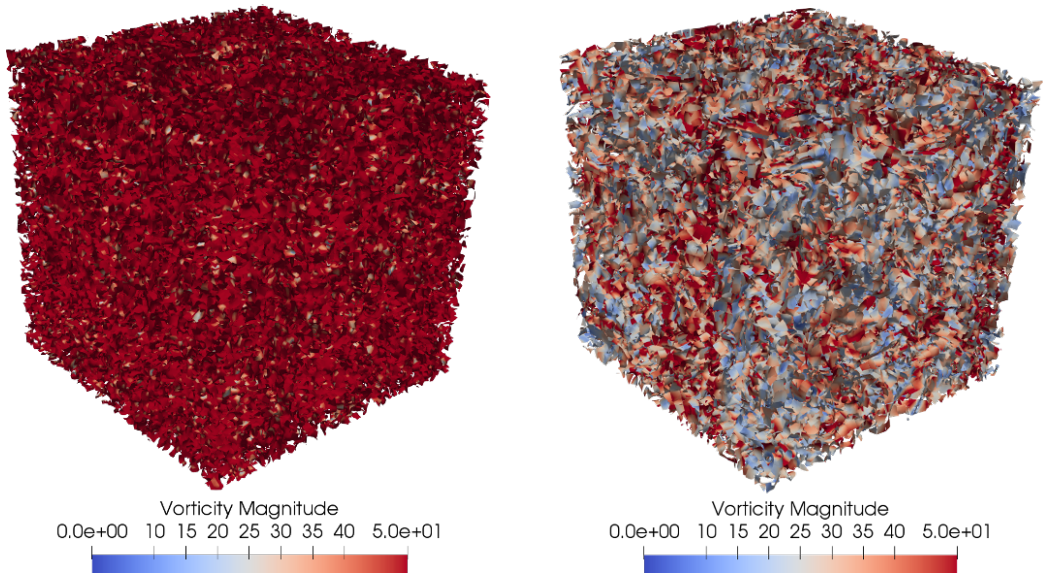

Figure 1: DIT. Isosurface of Q-criterion coloured with vorticity magnitude contours at $t^+ = 42$ (left) and $t^+ = 171$ (right), $\mathbb{P}^3$ solution approximation and 32^3 mesh

In the simulations, a cubic box $2\pi \times 2\pi \times 2\pi$ has been used as domain with periodic boundary conditions. The turbulent flow inside the domain moves along with the mean velocity of the flow. The initial solution consists of a random velocity field generated from the filtered experimental energy spectrum measured at the first station, *i.e.* at time $t^+ = tu/M = 42$, during the experiment. In fact, the experimental energy spectra have been filtered according to this equation to determine an initial velocity field for the computations, at $t^+ = 42$, and to compare the numerical results at $t^+ = 98$ and $t^+ = 171$. Figure 1 shows the isosurface of Q-criterion coloured with vorticity magnitude contours at $t^+ = 42$ (left) and $t^+ = 171$ (right) for a $\mathbb{P}^3$ solution approximation.

The simulations have been carried out on 32^3 cubic elements with linear edges with $\mathbb{P}^3$ solution approximation. The time-step has been set equal to $\Delta t^+ = 1.5$. The X-LES formulation has been used in pure LES mode, with the initial value of k given by

$$k = \frac{1}{\beta^*} \left(C_1 \Delta\right)^2 S. \tag{20}$$

The sensitivity to the model coefficient C_1 has been investigated, using three different values: 0.05, 0.06 and 0.07. As shown in Fig. 2, the numerical energy spectra at $t^+ = 98$ and $t^+ = 171$ obtained for $C_1 = 0.06$ are in good agreement with the filtered experimental energy spectra.

3.2 FLOW PAST A CIRCULAR CYLINDER AT $Re_\infty = 10^5$

The first testcase for the full formulation of X-LES is the unsteady flow around a circular cylinder at a Reynolds number Re $= 10^5$, based on the cylinder diameter d.

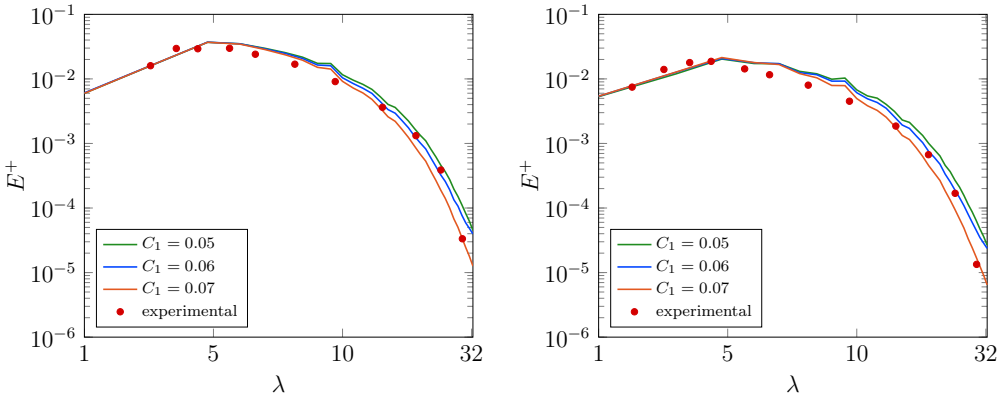

Figure 2: DIT. Filtered energy spectra at $t^+ = 98$ (left) and $t^+ = 171$ (right) for different model coefficient C_1, $\Delta = \frac{L}{32}$, 32^3 mesh, $\mathbb{P}^3$ solution approximation

The boundary layer is laminar until the separation, where the turbulent transition occurs immediately after the separation.

The flow is assumed to be periodic in the spanwise direction, with a period equal to twice the cylinder diameter. The mesh has 29630 hybrid elements, hexaedra in the boundary layer and prism outside, with quadratic edges. The 2D mesh (extruded in the third direction) has been generated with a high-order version of a fully automated in-house hybrid mesh generator based on the advancing-Delaunnay strategy [10]. The far-field boundary is at 20 chords. The elements in circumferential direction are 60 and in span-wise direction are 10, where the non-dimensional distance of the first mesh line from the wall is equivalent to $y_1^+ \sim 1$. The mesh shows a refinement in the wake area, where X-LES should be in the LES formulation. The mesh density near $(x/d, y/d) = (0.75, 0.5)$ is 6×10^{-2}, two times coarser than the resolution used by Kok *et al.* in [1] and by Travin et al. [11] ($\sim 3 \times 10^{-2}$).

The filter width has been set to the value $\Delta = 10^{-3}$. Fig. 3 shows the isosurfaces of Q-criterion coloured with vorticity magnitude around the cylinder with X-LES and URANS equations. Notice that flow-field computed by the hybrid method shows chaotic three-dimensional turbulent structures, which are not present in the URANS solution.

Fig. 4 shows the pressure coefficient, C_P, along the cylinder and the time history of the lift, C_L, and drag, C_D coefficients on the average time interval ($\sim$ 20 vortex shedding). X-LES gives a substantial improvement over URANS results, which strongly underpredict the pressure, and are in good agreement with the experimental data by Fage and Falkner [12]. The computed mean value for $C_D = 1.12$ is in agreement with the experimental value reported by Fage and Falkner [12] ($C_d = 1.06$) and Achenbach [12] ($C_d = 1.18$).

The mean streamwise velocity along the centreline of the cylinder and the mean cross-flow velocity profile at $x/D = 1$ are shown in Fig. 5 and compared with experimental data of Tremblay [13] (corresponding to a Reynolds number $Re = 1.4 \times 10^5$).

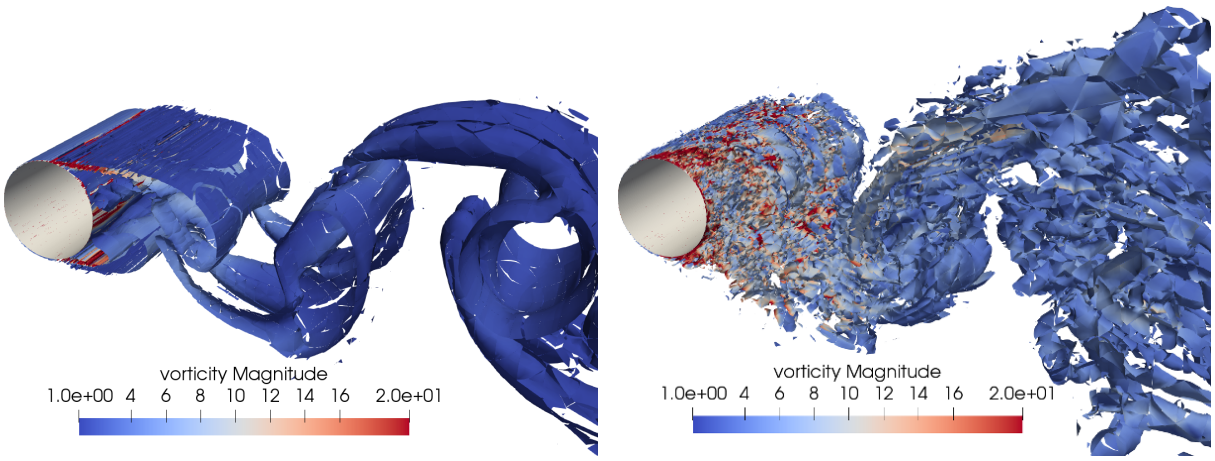

Figure 3: Cylinder. Isosurface of Q-criterion coloured with vorticity magnitude with $k-\omega$ (left) and X-LES (right), $\mathbb{P}^3$ solution approximation

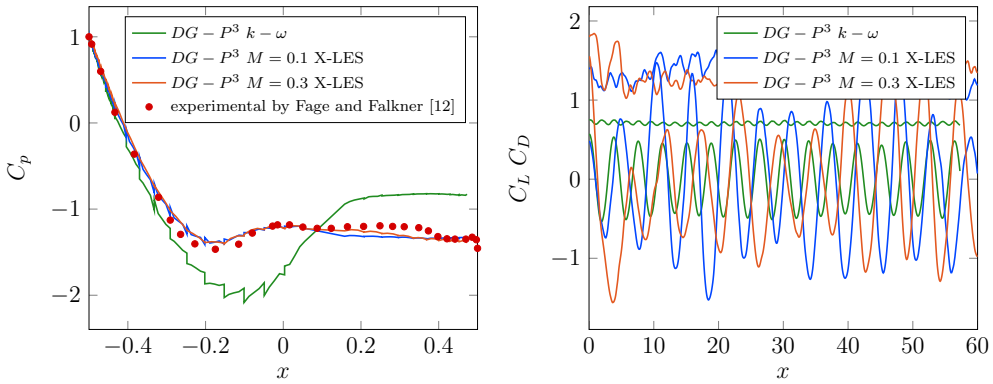

Figure 4: Cylinder. Pressure coefficient C_p (left) and lift and drag coefficient (right), $\mathbb{P}^3$ solution approximation

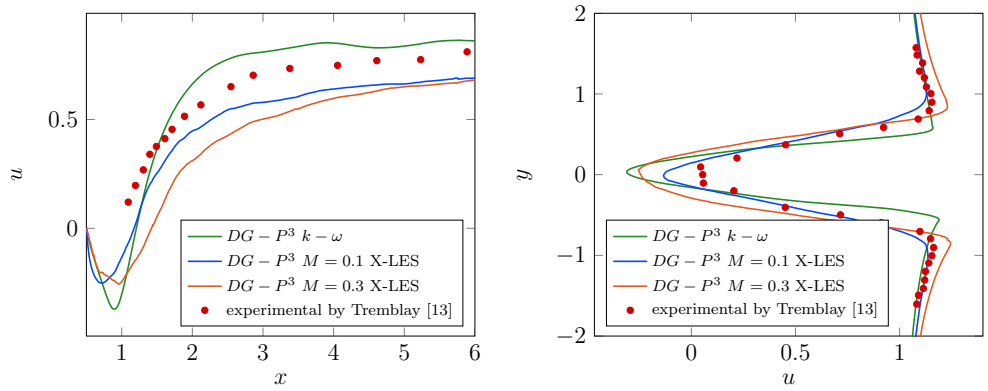

Figure 5: Cylinder. The mean streamwise velocity along the centreline of the cylinder (left) and the mean crossflow velocity profile at $x/D=1$ (right), $\mathbb{P}^3$ solution approximation

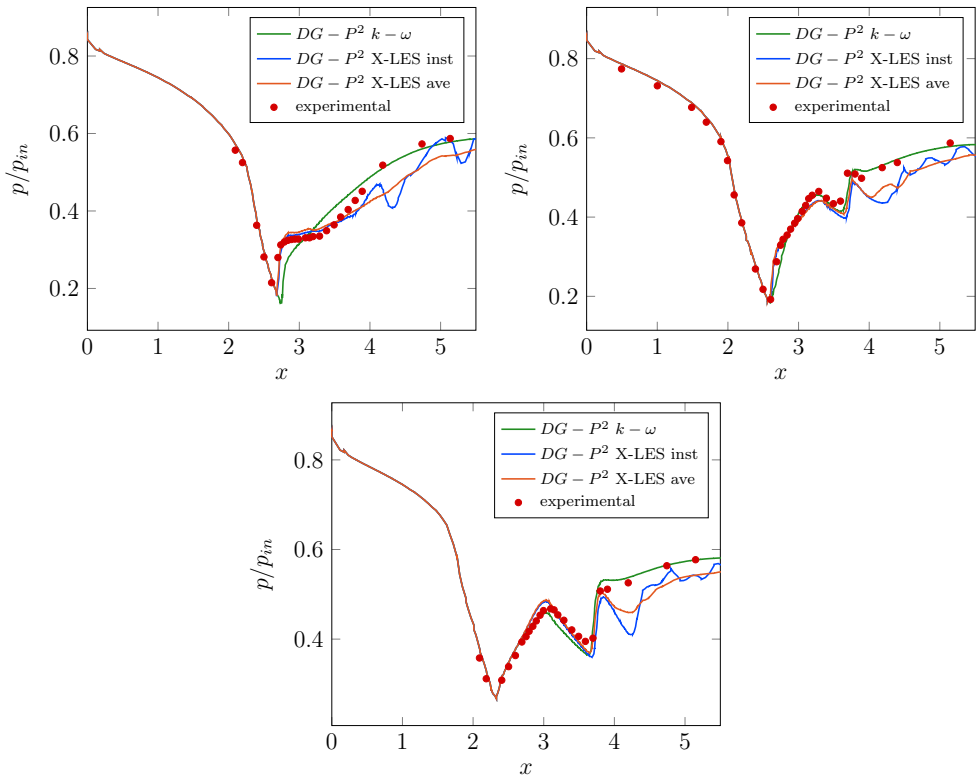

Figure 6: Transonic flow on a bump. p/p_{in} on the channel floor at $y = 0.15$, $y = 0.60$ and $y = 1.05$, $\mathbb{P}^2$ solution approximation

3.3 TRANSONIC FLOW IN A CHANNEL WITH A BUMP

In this section some preliminary results describing the X-LES model prediction capabilities in presence of shock waves are presented. In this problem the flow moves in a channel made of a converging diverging section with three flat faces and a swept bump on the lower wall [15]. The strong interactions between shocks and the boundary layers lead to the formation of several flow separations that generate complex vortical structures and secondary flows. The solutions have been computed for the following inlet conditions: $M = 0.75$ and $Re_H = 1.13{\times}10^6$. Results have been compared with experimental data [14] and a DG solution based on a "standard" RANS model. Computations have been performed up to $\mathbb{P}^2$ polynomial approximation on a 72 960 hexahedral elements mesh with quadratic edges. X-LES has been accurately integrated in time with the ROS3P scheme and a fixed filter width value $\Delta = 5e-2$. The pressure distribution on the floor at different sections of the channel are shown and compared with RANS and experiments in Fig. 6. Although significant differences between the RANS and X-LES Mach contours are observed in Figure 7, both the models are able to reasonably predict the shocks positions. In particular X-LES seems to predict slightly better the first shock location although some spurious oscillation, probably due to the boundary condition imposition, are observed at the channel outlet.

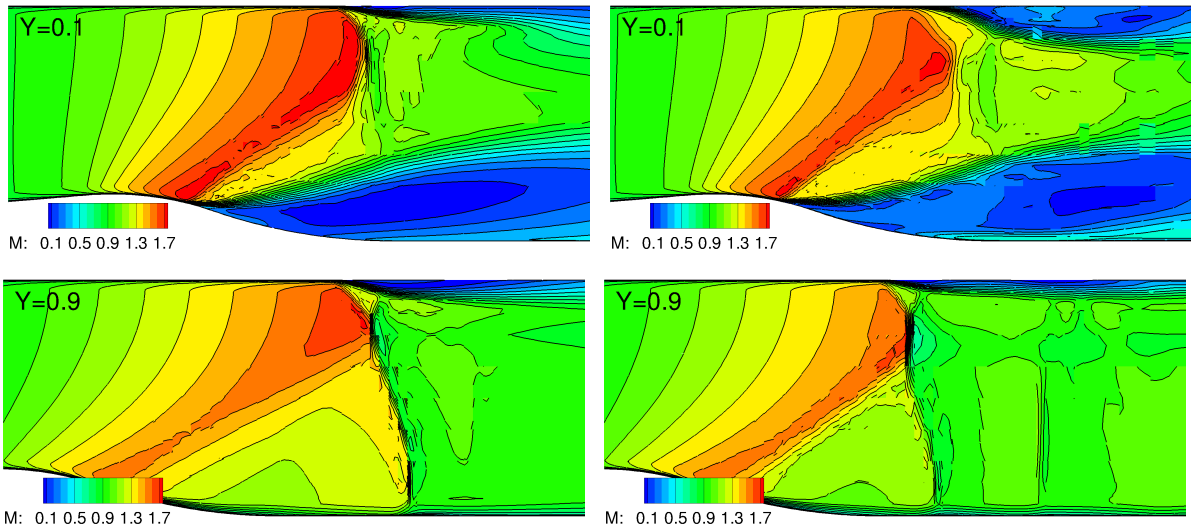

Figure 7: Transonic flow on a bump. $k-\omega$ (left) and X-LES (right) at $y = 0.1$ and $y = 0.9$

4 CONCLUSIONS

This work shows recent developments and applications of eXtra-Large Eddy Simulation (X-LES) model in the discontinuous Galerkin (DG) solver named MIGALE. The LES formulation of the X-LES method has been validated and recalibrated using the decay of homogeneous and isotropic turbulence (DHIT). The sensitivity of the energy spectrum to X-LES model constants and mesh size has been evaluated. The X-LES prediction capabilities have been demonstrated in the computation of external aerodynamic problems with massively separated flows, *i.e.* the flow around a circular cylinder at $\mathrm{Re} = 10^5$ and the shock wave/boundary layer interaction on a swept bump.

The performance, in terms of accuracy and computational efficiency, have been compared with RANS model and experimental data. In the framework of the adopted DG method, X-LES method proved to be robust and able to correctly deal with separated flows, improving the predicting capabilities over RANS model.

Work is in progress to extend the application of the hybrid method to other unsteady test cases, possibly considering problems of industrial relevance, and to move towards very-large scale parallel computations (ten of thousands cores).

5 ACKNOWLEDGMENTS

We acknowledge Dr. J.C. Kok at NLR for the suggestions on X-LES validation and for sharing the code for the DIT initial field generation. We acknowledge Dr. Michael Shur at SPBSTU for sharing the DIT initial field generation and post-processing tool. We acknowledge Dr. Werner Haase for sharing details on the DIT testcase adopted during some EU projects.

We acknowledge the CINECA and the Regione Lombardia award under the LISA initiative 2016-2018, for the availability of high performance computing resources and support within the projects "X-LES for TRAnsonic flows using the Discontinuous Galerkin

method" (HPL13PWPGF). Part of the results have been also achieved using the PRACE Research Infrastructure resource MARCONI-KNL based at CINECA, Casalecchio di Reno, Italy, within the Project "Discontinuous Galerkin method for the X-LES of TRAnsonic flows" (DGXTRA).

REFERENCES

[1] Kok, J. and Dol, H. and Oskam, B. and Van der Ven, H., *Extra-Large Eddy Simulation of Massively Separated Flows*, 42nd AIAA Aerospace Sciences Meeting and Exhibit, merican Institute of Aeronautics and Astronautics, 2004.

[2] Bassi, F. and Botti, L. and Colombo, A. and Crivellini, A. and Ghidoni, A. and Massa, F., *On the development of an implicit high-order Discontinuous Galerkin method for DNS and implicit LES of turbulent flows*, European Journal of Mechanics - B/Fluids, 2015.

[3] Bassi, F. and Botti, L. and Colombo, A. and Crivellini, A. and Ghidoni, A. and Nigro, A. and Rebay, S., *Time integration in the Discontinuous Galerkin code MIGALE - Unsteady problems*, IDIHOM: Industrialization of high-order methods - A top-down approach, Springer International Publishing, 2015.

[4] Bassi, F. and Botti, L. and Colombo, A. and Crivellini, A. and Ghidoni, A. and Nigro, A. and Rebay, S., *On the development of an implicit high-order Discontinuous Galerkin solver for a hybrid RANS-LES model*, DLES11 proceeedings, Springer International Publishing, 2018.

[5] Yoshizawa, A. and Horiuti, K., *A Statistically-Derived Subgrid-Scale Kinetic Energy Model for the Large-Eddy Simulation of Turbulent Flows*, Journal of the Physical Society of Japan, 1985.

[6] Lang, J. and Verwer, J., *ROS3P—An accurate third-order Rosenbrock solver designed for parabolic problems*, BIT Numerical Mathematics, 2001.

[7] Bassi, F. and Botti, L. and Colombo, A. and Ghidoni, A. and Massa, F., *Linearly implicit Rosenbrock-type Runge–Kutta schemes applied to the Discontinuous Galerkin solution of compressible and incompressible unsteady flows*, Computers & Fluids, 2015.

[8] Comte-Bellot, G. and Corrsin, S., *The use of a contraction to improve the isotropy of grid-generated turbulenc*e, Journal of Fluid Mechanics, 1966.

[9] Satish Balay and Shrirang Abhyankar and Mark F. Adams and Jed Brown and Peter Brune and Kris Buschelman and Lisandro Dalcin and Victor Eijkhout and William D. Gropp and Dinesh Kaushik and Matthew G. Knepley and Lois Curfman McInnes and Karl Rupp and Barry F. Smith and Stefano Zampini and Hong Zhang, *PETSc Users Manual*, Argonne National Laboratory, 2015.

[10] Ghidoni, A. and Pelizzari, E. and Rebay, S. and Selmin, V., *3D anisotropic unstructured grid generation*, International Journal for Numerical Methods in Fluids, 2006.

[11] Travin, A. and Shur, M. and Strelets, M. and Spalart, P. R., *Physical and Numerical Upgrades in the Detached-Eddy Simulation of Complex Turbulent Flows*, Advances in LES of Complex Flows: Proceedings of the Euromech Colloquium 412, Springer Netherlands, 2002.

[12] Achenbach, E., *Distribution of local pressure and skin friction around a circular cylinder in cross-flow up to* $\mathrm{Re} = 5 \times 10^6$, Journal of Fluid Mechanics, 1968.

[13] Tremblay, F., *Direct and large eddy simulation of ow around a circular cylinder at sub critical Reynolds numbers*, Technische Universität München, 2001.

[14] Délery J., and Marvin J.G., *Shock wave/boundary layer interaction*, AGARDograph No 280, June 1986.

[15] Cahen J., Couaillier V., Délery J., and Pot T., *Validation of code using turbulence model applied to three-dimensional transonic channel*, AIAA Journal, Vol. 33, No 4, P. 671-679 1995.